ELSEVIER

Journal of Marine Systems 21 (1999) 379–397

JOURNAL OF MARINE SYSTEMS

Dissection of the GHER turbulence closure scheme

Eric J.M. Delhez *, Marilaure Grégoire [1], Jacques C.J. Nihoul, Jean-Marie Beckers [2]

GeoHydrodynamics and Environment Research Lab., University of Liège, Sart Tilman B5, B-4000 Liège, Belgium

Received 10 December 1998; accepted 10 December 1998

Abstract

In this paper, the turbulence closure scheme implemented in the GHER hydrodynamic model is described in detail. Two case studies carried out in two contrasting conditions—one in the shallow, tide dominated, north-western European continental shelf, and the other in the deep Mediterranean Sea—are used to identify the dominant terms of the equation for the turbulent kinetic energy, first theoretically, secondly from the results of the simulations. In both domains, the dominant terms are the local destruction and production terms, the vertical diffusion term and to a smaller degree, the time derivative. Advection and horizontal diffusion turn out to be negligible in most of the relevant cases for such large scale studies. This opens the way to simplifications and optimisations of the numerical models.

Keywords: turbulence closure scheme; 3D hydrodynamic model; North Sea; Mediterranean Sea

1. Introduction

The impressive development of three-dimensional hydrodynamic models and environmental applications has highlighted the need of a proper parameterisation of turbulent fluxes in these mathematical models (e.g., Mellor and Yamada, 1982; Nihoul et al., 1989). While hydrodynamic models rely, for the largest part, on well-established laws and properties like Newton's law of dynamics and the conservation of mass of the different constituents, the modelling of the mean effect of sub-grid and sub-window scale processes on the mean flow described by the model is based on simplifying hypotheses on the structure and the mean effect of the turbulent fluctuations. The appropriateness of these hypotheses depending a priori on the application at stake and, in particular, on the spatial and time scale of the study, the design and/or choice of a turbulence closure scheme deserves a careful examination.

From a practical point of view, the numerical aspects, i.e., the CPU requirements, the expected accuracy of the scheme and the sensitivity of the whole modelled processes on the parameterisation of the turbulent fluctuations must also be taken into account in the decision as well as the availability of appropriate atmospheric forcing data. It is, for instance, widely accepted that simple algebraic turbulent closure schemes can be used to compute three-dimensional tidal flows (e.g., Davies and Jones, 1990; Davies et al., 1995) while refined, more demanding,

* Corresponding author. Fax: +32-4-366-2355; E-mail: e.delhez@ulg.ac.be

[1] Research Assistant at the National Fund for Scientific Research (Belgium).

[2] Research Associate at the National Fund for Scientific Research (Belgium).

0924-7963/99/$ - see front matter
PII: S0924-7963(99)00023-8

approaches are required to study the post bloom evolution of phytoplankton that depends crucially on the, even small, supply of nutrients from the bottom layer through the thermocline (e.g., Varela et al., 1992).

Turbulence closure schemes range from simple algebraic expressions,—relating the vertical eddy viscosity and diffusivity to the velocity—, to systems of one, two or more differential equations (e.g., Luyten et al., 1996) for characteristic quantities of the turbulence (turbulent kinetic energy per unit mass k, mixing length ℓ, dissipation rate of the turbulent kinetic energy ε, turbulent Reynolds stresses). Among these, $k-\ell$ and $k-\varepsilon$ models are more and more popular in the community of ocean modellers and are sometimes regarded as the ultimate solution to this issue (e.g., Rodi, 1980, 1987; Mellor and Yamada, 1982). There are still however some problems associated with the implementation of these schemes like their sensitivity to the forcing data and to the spatial resolution in space and time.

In practical applications, one cannot usually afford the high resolution required by $k-\varepsilon$ models (e.g., Burchard and Petersen, 1999) and more robust turbulence closure schemes may be useful. In this paper, we describe the turbulence closure used in the GHER hydrodynamic model (Nihoul et al., 1989), in which the mixing length is evaluated from simple inspection as a parametric algebraic expression, and try to show that k models are adequate for several hydrodynamic situations.

Despite the high level of parameterisation supporting turbulent closure schemes, these are also often regarded as black boxes by many. It is however desirable to be aware of the main processes behind the closure scheme, of the significance of the different terms (to introduce mathematical or numerical simplifications) and of sensitivity of the scheme to the parameters, the spatial discretisation or the meteorological forcing function. Therefore, some aspects of GHER closure scheme are examined in this paper.

2. General formulation of the GHER turbulence closure scheme

The turbulence closure scheme implemented in the GHER hydrodynamic model provides a parameterisation of the effects of turbulence based on Kolmogorov's theory. If one takes into account the relative orders of magnitude of horizontal and vertical variations, turbulent fluxes reduce to their vertical component—no account is given here of the horizontal turbulent fluxes associated with the subgrid scale processes that have to be introduced because of the limited spatial and temporal resolution of the numerical models even if similar principle can be used to derive their appropriate parameterisation (Ozmidov, 1967)—and can be expressed on the Fourier–Fick–Onsager model as:

$$\tilde{\phi}^{y} = -\tilde{\lambda}^{y}\frac{\partial y}{\partial x_3}\boldsymbol{e}_3 \tag{1}$$

for the vertical turbulent flux $\tilde{\phi}^{y}$ of a scalar property y like salinity, temperature, turbulent kinetic energy or any concentration, and:

$$\tilde{\phi}^{u} = -\tilde{\nu}\frac{\partial \boldsymbol{u}}{\partial x_3}\boldsymbol{e}_3 \tag{2}$$

for the vertical turbulent flux of momentum $\tilde{\phi}^{u}$, where $\tilde{\nu}$ and $\tilde{\lambda}^{y}$ are, respectively, appropriate eddy viscosity and eddy diffusivity, $\boldsymbol{u}$ is the horizontal velocity vector, x_3 is the vertical co-ordinate and $\boldsymbol{e}_3$ is the unit vertical vector (pointing upwards).

By dimensional arguments, the eddy diffusivity can be related to the total kinetic energy of the fluctuations, i.e., the turbulent kinetic energy, and to a characteristic spatial scale of the larger eddies, i.e., the mixing length ℓ, through the algebraic relation,

$$\tilde{\nu} = \alpha\,\ell\sqrt{k} \tag{3}$$

where $\alpha(\sim 0.5)$ is a dimensionless constant.

The evolution equation for k takes the usual form:

$$\frac{\partial k}{\partial t} + \boldsymbol{v}\cdot\nabla k = \Pi + \tilde{\nu}M^2 - \tilde{\lambda}^{b}N^2 - \varepsilon + \frac{\partial}{\partial x_3}\left(\tilde{\lambda}^{k}\frac{\partial k}{\partial x_3}\right) + \mathscr{D}(k) \tag{4}$$

expressing that the rate of change of k observed locally is due to the advection by the mean flow, to the local production at the Prandtl frequency:

$$M^2 = \nabla\boldsymbol{v}:\nabla\boldsymbol{v} \sim \frac{\partial \boldsymbol{u}}{\partial x_3}\cdot\frac{\partial \boldsymbol{u}}{\partial x_3} \tag{5a}$$

(taking into account that vertical gradients are much greater than horizontal ones while vertical velocities are much smaller than the horizontal ones $\boldsymbol{u}$), to the inhibition of turbulence by the stratification operating at the Brunt–Väisälä frequency:

$$N^2 = \frac{\partial b}{\partial x_3} \tag{5b}$$

where b is the buoyancy, to the local dissipation of k at the dissipation rate ε:

$$\varepsilon = (\alpha k^{1/2})^3 \ell^{-1} \tag{6}$$

and to the vertical turbulent diffusion of k characterised itself by a turbulent diffusivity coefficient $\tilde{\lambda}^k$. The extra term Π is introduced to account for the production of turbulent kinetic energy by unresolved processes like mesoscale oscillations, waves (e.g., Kitaigorodskii, 1979; Beckers, 1991). The notation $\mathscr{D}(k)$ is used to represent horizontal diffusion.

While $k-\ell$ and $k-\varepsilon$ type models introduce an evolution equation for ε or ℓ, the system of Eqs. 1–6 is closed in the current approach by providing an algebraic parametric expression for ℓ:

$$\ell = \ell_0(x_3)\,\psi(R_f) \tag{7}$$

where

$$\ell_0 = \min\left\{\kappa(x_3+h)\left(1-\delta\frac{x_3+h}{H}\right), \ell_{\max}\right\} \tag{8}$$

is the mixing length in neutral stability conditions and $\ell_{\max}$ its maximum value, where:

$$\psi(R_f) = 1 - \frac{R_f}{R_{f_c}} \tag{9}$$

is a decreasing function of the Richardson flux number R_f:

$$R_f = \frac{\tilde{\lambda}^b N^2}{\Pi + \tilde{\nu} M^2} \tag{10}$$

used to reflect the flattening of eddies under stable stratification (h is the reference depth, $H = \zeta + h$ is the total depth, ζ is the free surface elevation above the reference level ($x_3 = 0$), $\kappa = 0.4$ is the von Karman's constant. $\delta \in [0.5, 1]$ is a dimensionless variable parameter used to adapt the mixing length profile to the surface conditions, $R_{f_c} \in [0.2,1]$ is the critical Richardson flux number).

From the previous expressions, the eddy viscosity can be computed by Eq. 3 while eddy diffusivity coefficients are given by:

$$\tilde{\lambda}^y = \beta^y \tilde{\nu} \tag{11}$$

where the β^y, inverse of the turbulent Schmidt numbers, depend also on the stratification to take into account the stronger negative influence of stratification on the turbulent exchange of heat, salt... than on turbulent exchange of momentum :

$$\beta^b = \beta^T = \beta^S = \gamma\sqrt{1 - \frac{R_f}{R_{f_c}}} \tag{12}$$

$$\beta^u = \beta^k = 1 \tag{13}$$

where $\gamma(=1.1)$ is a constant.

The reasons behind the simplification of leaving out the additional evolution for ℓ or ε and replacing it by algebraic expressions are easily understandable. While the equation for k is widely accepted and suffers few simplifications or hypotheses, equations for ℓ or ε cannot be written without rather limiting hypotheses on the characteristics of the turbulent fluctuations or largely empirical approaches. In many situations however, and particularly in shallow shelf seas where the water column seldom splits in more that two layers, suitable representation of ℓ can be obtained so that it is preferable to avoid the additional complexity and CPU cost induced by the evolution for ℓ or ε and use formulae like Eqs. 7–8.

It is interesting to remark that such a prescribed mixing length profile is also present in Mellor and Yamada's approach. The purpose of the so-called 'wall proximity function' introduced in the dissipation rate of $k\ell$ is indeed to relax the computed mixing length towards a fixed profile that satisfies the law of the wall at the bottom (e.g., Deleersnijder and Luyten, 1994). One can regret that the same asymptotic behaviour is assumed at the surface as if it were a solid boundary.

The scheme is complemented by appropriate boundary conditions for k. At lateral solid boundaries, both the advection and diffusion fluxes are

zero. At the open boundaries, Eq. 4 is solved by dropping all horizontal derivatives. In shallow seas and regions of large depth gradients, a large turbulence input occurs through the friction of currents on the rough bottom. The precise dynamics of this generation mechanism cannot generally be represented in a 3D model unless a prohibitively fine vertical grid spacing is used to describe the bottom friction layer in detail. A logarithmic bottom boundary layer can however be assumed and the level of turbulent kinetic energy at the bottom is therefore computed assuming local equilibrium between the production and destruction terms of k:

$$k_e = \frac{u_*^2}{\alpha^2} \tag{14}$$

where u_* is the friction velocity. At the surface, the same approach can be applied or the turbulence input from the wind field can be prescribed according to:

$$\lambda^k \frac{\partial k}{\partial x_3}\bigg|_{x_3=\zeta} = \frac{1}{\rho_0} C_k \|\tau_w\|^{3/2} \tag{15}$$

where ρ_0 is the seawater density and τ_W is the wind stress.

3. Applications

The GHER hydrodynamic model (Nihoul, 1993) has been successfully applied in many marine areas around the world: Bering Sea (Deleersnijder and Nihoul, 1988), North Sea (Martin and Delhez, 1994), Mediterranean Sea (Beckers, 1991), Black Sea (Grégoire et al., 1998)... demonstrating the generality of the approach. In this section, the relevant particularities of some implementations are described.

3.1. North-western European continental shelf

The north-western European continental shelf includes the marginal seas around the British Isles: North Sea, English Channel, Irish Sea. It is a relatively shallow shelf: the depth is smaller than 200 m everywhere except along the Norwegian Coast and even smaller than 100 m for the largest part.

The friction of the large tidal and storm surge currents on the bottom induces high levels of turbulence in the shallowest parts like the Southern Bight of the North Sea or the Eastern English Channel (Fig. 1) so that the water column remains well-mixed during the whole year. In less shallow areas, like the Central and Northern North Sea, the Celtic Sea and the shelf break region, the tidal mixing is not strong enough to oppose the solar heating. The thermal stratification develops, therefore, during spring as a result of the reduction of the wind energy input and remains present until the end of the summer (with a variation of the depth and strength of the thermocline). This stratification induces a further reduction of the level of turbulence as does the persistent,—variable in strength—, haline stratification along the Norwegian Coast.

The turbulent kinetic energy contours in Fig. 1 delineate the limits of the stratified and well-mixed regions and can be used to identify the well-known tidal fronts like the Flamborough Head's front in the Southern North Sea, the Ushant front in the English Channel or the complex thermal structure in the Irish Sea.

The GHER model is used to study the hydrodynamics from time scales of a few hours to a full year. At the smaller time scales, the emphasis is on the accurate prediction of water levels and tidal currents while the simulation of the long term fate of pollutants and the dynamics of nutrients is the focus of the studies carried out at larger time scales.

In the implementation considered here, the model covers the whole shelf with an horizontal resolution of 10′ in longitude and latitude (i.e., about 12×18 km) and 10 vertical σ-levels. It is forced with six hourly wind stress and heat fluxes from the ECMWF, with 10 tidal components at the open boundary with the Atlantic and with the discharge of the 30 most important rivers in the area.

3.2. Mediterranean Sea

The GHER model was applied to the Mediterranean Sea at seasonal scale. Contrary to the north-western European continental shelf, the Mediterranean Sea is an almost closed basin without noticeable tidal effects except in particular, limited, locations. As a concentration basin, it presents some particular processes needed to assure mass and salt balances. Deep water formations take indeed place and lead to strong vertical mixing in the Gulf of

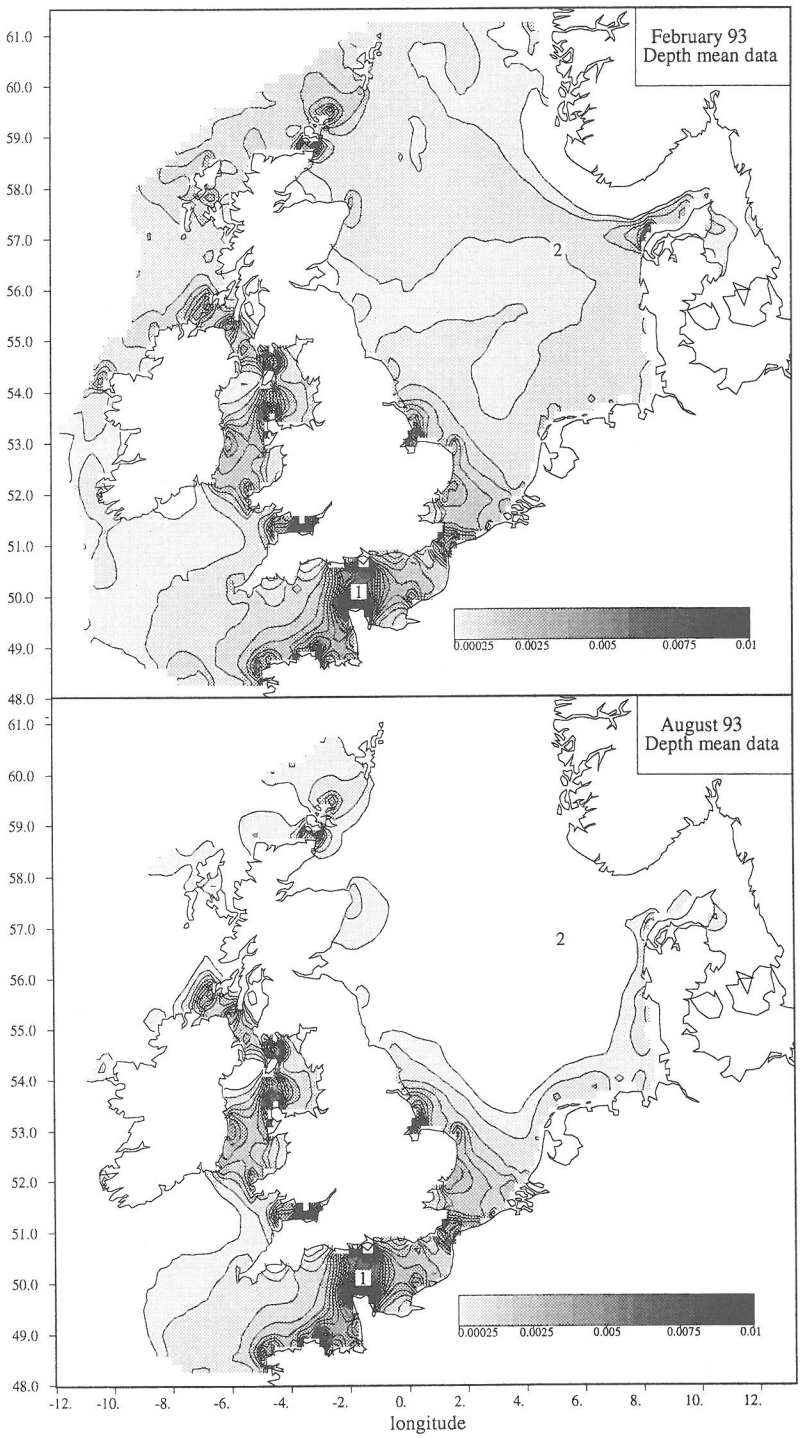

Fig. 1. Depth averaged turbulent kinetic energy (m^2/s^2) on the north-western European continental shelf averaged for February 1993 (top panel) and August 1993 (bottom panel). The labels 1–2 indicate the locations of points N1 and N2 (see Fig. 5).

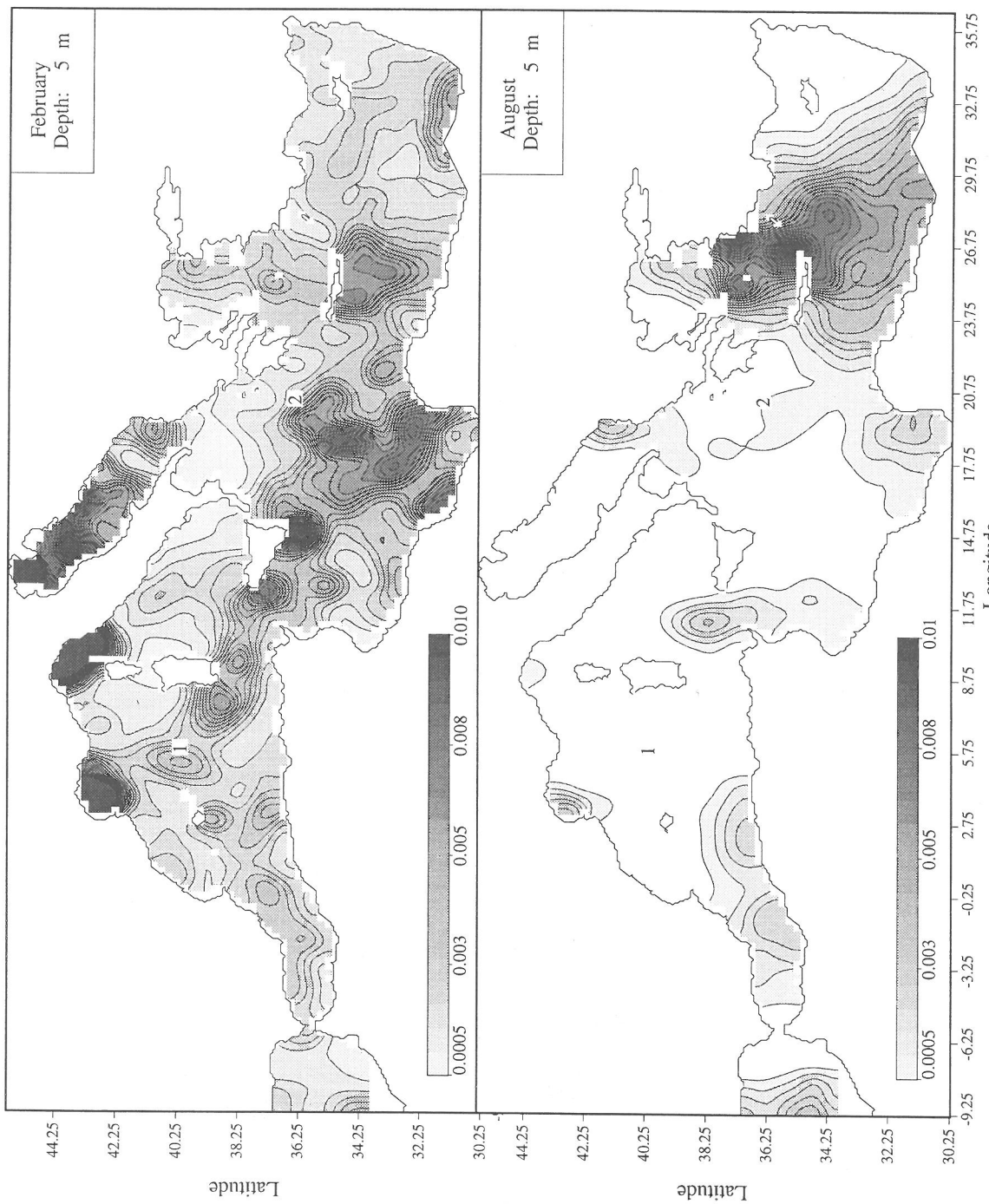

Fig. 2. Turbulent kinetic energy (m^2/s^2) at 5 m depth in the Mediterranean Sea averaged for February (top panel) and August (bottom panel). The labels 1–2 indicate the locations of points M1 and M2 (see Fig. 6).

Lions (North western Mediterranean), the Adriatic sea and the Levantine basin in the eastern Mediterranean. Except these strong mixing events, the Mediterranean exhibits a rather well-defined stratification, maintaining three different overlaying water masses (the modified Atlantic waters in the surface layers, the Levantine intermediate waters at 200–400 m depth and the deep waters below). Between these water masses, vertical exchanges are small and the Mediterranean may be regarded as a 'miniature ocean', very different from the tidally dominated north-western European Continental Shelf.

The model applied to the Mediterranean was forced by daily ECMWF wind-stress and heat fluxes covering the period of 1978–1993. Salinity fluxes were based on a blending of ECMWF evaporation values, climatological precipitation fields of Jaeger (1976) and a small surface relaxation towards climatological sea surface salinity from the MODB data base (Brasseur et al., 1996).

The model is setup on a $1/4°$ (i.e., 22×26 km) grid with 31 vertical levels, initialised with the MODB T,S climatological winter fields and run for the 15 year period covered by the ECMWF data, with an Atlantic box in which a relaxation towards climatological seasonal cycles is maintained.

The model response to this forcing exhibits a clear seasonal cycle and conforms to the classical view of the Mediterranean circulation. Here, we will not describe the results of the model in terms of circulation and hydrography, but will concentrate on the modelled turbulence.

For details on the modelling of the Mediterranean circulation, we refer to the model intercomparison described in (Beckers and MEDMEX, 1998), where it is shown that the models (MOM, POM, OPA, GHER) represent the general circulation relatively well and that the most important parameter for the model calibration is the vertical diffusion coefficient (several models still use a constant vertical diffusion coefficient, which needs of course an ad hoc calibration).

Our present analysis is, thus, concentrating on turbulent aspects. From an inspection of the turbulent kinetic energy calculated by the model, it is rapidly seen that below the mixed surface layer, the turbulent kinetic energy drops by several orders of magnitude. This corresponds to the classical view of a deep ocean void of turbulence compared to the surface layer (and in some regions the bottom layer).

Only when deep-water formation takes place, is some turbulence found in the deeper parts. As seen from Fig. 2, turbulence levels are highest in the regions with stronger currents (as along the African coast), or strong wind fields and weaker stratification (as in the Gulf of Lions, the Aegean and the Adriatic), something we may anticipate. It is also seen that the summer stratification even more concentrates the turbulence in the surface.

4. Diagnosis of the k-equation

In the formulation of Eq. 4 local variations of the turbulent kinetic energy can result from five different processes, i.e., advection by the mean flow, net local production, local dissipation, horizontal diffusion and vertical diffusion. To get a better insight into the dynamics of turbulence, it is interesting to examine the relative contribution of these different processes in the budget of k.

To do so, let us first number the different terms of Eq. 4 according to:

$$d_1 = \frac{\partial k}{\partial t}$$

$$d_2 = \boldsymbol{v} \cdot \nabla k$$

$$d_3 = \Pi + \tilde{\nu} M^2 - \tilde{\lambda}^b N^2$$

$$d_4 = \varepsilon$$

$$d_5 = \mathscr{D}(k) = \nabla_h \cdot (K_h \nabla_h k)$$

$$d_6 = \frac{\partial}{\partial x_3}\left(\tilde{\lambda}^k \frac{\partial k}{\partial x_3}\right) \qquad (16)$$

where K_h is the horizontal diffusion coefficient of k. The order of magnitude of the different terms can be expressed as:

$$d_1 \sim \frac{k}{t_c}$$

$$d_2 \sim \frac{Uk}{L_h}$$

$$d_3 \sim \alpha \ell \sqrt{k}\, M^2 (1 - R_f) \sim \alpha \ell \sqrt{k} \left(\frac{U}{L_v}\right)^2 (1 - R_f)$$

$$d_4 \sim \frac{\alpha^3 k^{3/2}}{\ell}$$

$$d_5 \sim \frac{K_H k}{L_h^2}$$

$$d_6 = \frac{\alpha \ell k^{3/2}}{L_v^2} \tag{17}$$

where t_c is a characteristic time scale of variations of k, U is a characteristic horizontal velocity, L_h and L_v are characteristic horizontal and vertical length scales. We can then proceed with the magnitude analysis by comparing the different terms with respect to the dissipation rate d_4.

The processes resolved in the large scale northwestern European continental shelf model considered here have horizontal length scales $L_h \geq 10^4$–10^5 m and time scales $t_c \geq 10^4$ s (the tidal and/or meteorological forcing functions used do not introduce smaller time scales and mesoscale oscillations are hardly described). One has also $U \sim 0.5$ m/s and $K_h \sim 10^3$ m^2/s. One comes therefore up with the following ratios:

$$d_1/d_4 \sim \frac{\ell}{\alpha^3 t_c \sqrt{k}} \leq 10^{-3} \frac{\ell}{\sqrt{k}}$$

$$d_2/d_4 \sim \frac{U\ell}{\alpha^3 L_h \sqrt{k}} \leq 10^{-3} \frac{\ell}{\sqrt{k}}$$

$$d_5/d_4 \sim \frac{K_h \ell}{\alpha^3 L_h^2 \sqrt{k}} \leq 10^{-4} \frac{\ell}{\sqrt{k}}$$

$$d_6/d_4 \sim \left(\frac{\ell}{\alpha L_v}\right)^2. \tag{18}$$

Assuming that the dominant balance in Eq. 4 is between the net production and dissipation terms, the magnitude of k is given by:

$$d_3 \sim d_4 \Rightarrow k \sim \left(\frac{U\ell}{\alpha L_v}\right)^2 (1 - R_f). \tag{19}$$

This is, a priori, a reasonable assumption as turbulence must be produced before being advected or diffused and will always be eventually dissipated.

Therefore,

$$\frac{\ell}{\sqrt{k}} \sim \frac{\alpha L_v}{U\sqrt{1 - R_f}} \tag{20}$$

and

$$d_1/d_4 \leq \frac{L_v}{\alpha^2 U t_c \sqrt{1 - R_f}}$$

$$d_2/d_4 \leq \frac{L_v}{\alpha^2 L_h \sqrt{1 - R_f}}$$

$$d_5/d_4 \sim \frac{K_h L_v}{\alpha^2 U L_h^2 \sqrt{1 - R_f}}$$

$$d_6/d_4 \sim \left(\frac{\ell}{\alpha L_v}\right)^2. \tag{21}$$

In non stratified regions, the vertical length scale can be estimated as some proportion of the total depth $L_v \sim \theta H$, where $\theta = O(0.1)$ while the mixing length behaves asymptotically as κz at the bottom and, according to Eqs. 7–8 satisfies:

$$\ell \leq \min\left(20\,\text{m}, \frac{\kappa H}{4\delta} \sim 0.1 H\right), \tag{22}$$

therefore, for depths from meters to tenths of meters, say $H \sim 10$ m,

$$d_1/d_4 \sim 10^{-3}$$

$$d_2/d_4 \sim 10^{-4} - 10^{-3}$$

$$d_5/d_4 \sim 10^{-6} - 10^{-4}$$

$$d_6/d_4 \sim 10^{-1} - 10^{-2}. \tag{23}$$

This scaling is in agreement with the assumption of local equilibrium and shows that:

- horizontal diffusion is always negligible,
- horizontal advection is negligible in the coarse grid models considered in this paper, as also shown in (Ruddick et al., 1995),
- the importance of the time derivative, advection and diffusion terms increases with H, while the

relative importance of the vertical diffusion decreases with H,
- near the thermocline, where both the vertical length scale and the mixing length decrease severely as R_f increases, this analysis will presumably have to be refined,
- when the typical spatial length scale of the flow is larger than the mixing length, the vertical diffusion can be neglected. On the contrary, for regions with strong gradients, the vertical diffusion of k acts more rapidly and the local adjustment must be corrected for the vertical diffusion.

A similar conclusion can be drawn from the analysis of the behaviour of small perturbations around the local equilibrium value k_e such that:

$$\tilde{\nu} M^2 (1 - R_f) = \frac{\alpha^4 k_e^2}{\tilde{\nu}}, \tag{24}$$

i.e.,

$$k_e = \frac{1}{\alpha^2} \ell^2 M^2 (1 - R_f). \tag{25}$$

If the spatial derivatives are neglected, the law governing the adaptation towards the equilibrium for small perturbations in a fixed density fields is:

$$\frac{\partial k'}{\partial t} = \frac{\sqrt{k_e + k'}}{\ell} \left[\alpha \ell^2 M^2 (1 - R_f) - \alpha^3 (k_e + k') \right]$$

$$\approx - \frac{\alpha^2 \tilde{\nu}}{\ell^2} k'. \tag{26}$$

This shows that the time-scale for local adjustment is given by $\alpha^{-2} \ell^2 \tilde{\nu}^{-1}$. Comparing this result with the time scale for vertical diffusion, $L_v^2 / \tilde{\nu}$, one can see that the vertical diffusion acts more slowly for regions with low gradients ($L_v \gg \ell$) and can thus be neglected when the typical spatial length scale of the flow is larger than the mixing length. Since, in most cases, the mixing length is also a measure of the typical length scale of mixing, and hence of the gradients, we expect that, in general, there will be a situation where vertical diffusion and local adjustment act together on turbulent fields.

A similar analysis of the orders of magnitude can be done for the Mediterranean Sea Model. The parameters must then be adapted to the characteristics of the region and of the model, i.e.,

$$L_h \sim 10^5 \text{ m}$$

$$L_v \sim 5 \cdot 10^1 \text{ m}$$

$$t_c \sim 10^5 - 10^6 \text{ s}$$

$$U \sim 0.1 \text{ m/s}$$

$$K_h \sim 2\,10^2 \text{ m}^2/\text{s}. \tag{27}$$

The scaling of the different terms is then:

$$d_1 / d_4 \sim 5 \cdot 10^{-3}$$

$$d_2 / d_4 \sim 5 \cdot 10^{-4}$$

$$d_5 / d_4 \sim 10^{-6}$$

$$d_6 / d_4 \sim 10^{-1} \tag{28}$$

supporting similar conclusions.

4.1. Numerical verification

To clarify the previous theoretical developments, the same analysis was carried out with results of the GHER models of the north-western European Continental Shelf and the western Mediterranean Sea.

We can introduce a suitable norm of the different terms by defining $\langle d_i \rangle$ as the monthly average (or over any suitable period of time for the measure to be statistically meaningful) of the absolute value of d_i. Since turbulent fields are spatially very inhomogeneous, it is desirable to normalise these $\langle d_i \rangle$ in order to be able to compare the dynamics of k at different locations. We then define:

$$D_i = \log \left(\frac{2 \langle d_i \rangle}{\sum_j \langle d_j \rangle} \right). \tag{29}$$

This scaling is chosen so that, when the equation for k reduces to a balance between two dominant terms, each of them has a scaled measure of zero and the other ones are negative numbers. In this case, D_i can be considered as the order of approximation for which the term d_i has some influence on the dynamics.

Figs. 3 and 4 show the results of the horizontal distribution of these gauges. It should be mentioned that the estimates $\langle d_i \rangle$ were evaluated in a way that is fully coherent with the integration scheme taking

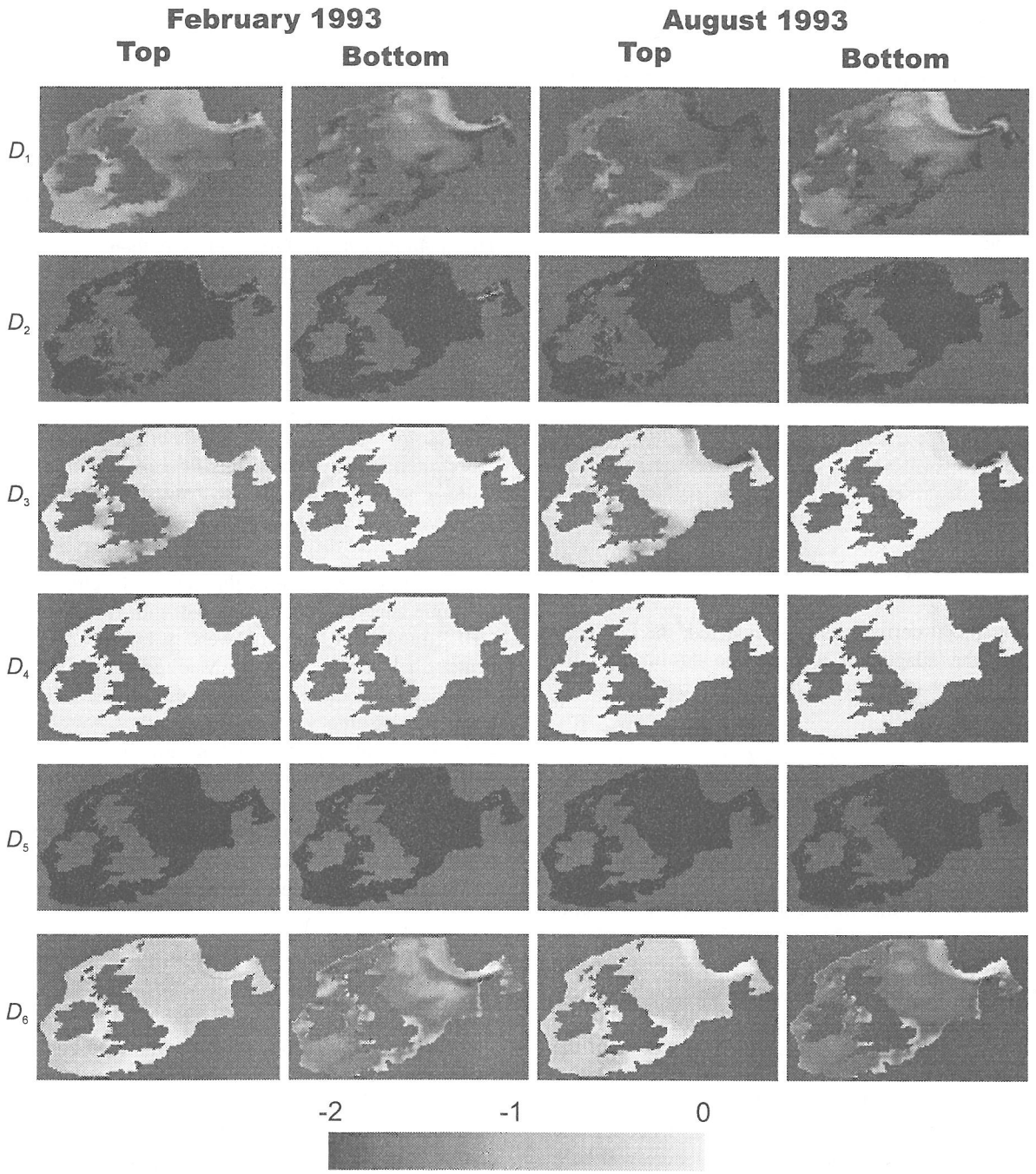

Fig. 3. Horizontal distributions, at the surface and at the bottom, of the norms of the different terms involved in the equation of k on the north-western European continental shelf in February and August 1993.

into account that some terms (the dissipation rate and the vertical fluxes) are actually computed with some level of implicity. Fig. 3 shows the surface and bottom distributions of the normalised estimates D_i on the north-western European Continental Shelf for February and August 1993, i.e., respectively for well-mixed and partly stratified conditions. Fig. 4a–b show the same gauges at three different depths and two different dates in the Mediterranean Sea.

As assumed in the theoretical analysis, the dominant balance is clearly between the net production d_3, dissipation d_4 and diffusion d_6 terms at the two sites. A smaller contribution comes also from the temporal derivative d_1. Horizontal diffusion d_5 and advection by the mean flow d_2 have, on the contrary, no significant influence of the budget. It is remarkable that the same conclusions are reached in the two very different sites studied. The reasons for this are however obvious: both study concentrate on the large scale circulation at mesoscale or larger time scales.

A more careful examination of the plots, complemented with the vertical profiles shown in Figs. 5 and 6 reveals further similarities but also some dissimilarities.

The importance of the vertical diffusion is ostensibly larger in the Mediterranean Sea results than in the north-western European continental shelf. This is a consequence of the different dynamics of the two regions.

In the Mediterranean Sea, turbulence may be produced by local features like baroclinic instabilities of frontal currents, gravity currents, breaking of internal waves, etc. In most part of the Mediterranean Sea, however, turbulence is only produced by the wind stress at the surface,—especially in the numerical models as many of the small scale processes leading to the production of the turbulence are very poorly resolved, if present, in the large scale models. This forcing function contributes to the generation of turbulence both directly by the flux of turbulent kinetic energy from the wind field to the sea (this flux accounts also for the strong wave and shear production in the very top layer that cannot be resolved by the model) and indirectly by the production associated with the velocity shear in the surface layer. From the different plots, one can infer that the former contribution is the dominant one close to the surface. This results in a downward diffusion flux of turbulent kinetic energy and the progressive decrease of the turbulence level as dissipation dominates over production. The maximum of turbulence is thus found at the surface and the distributions of k at different depths are rather similar. Below the thermocline, however, the surface signal can be hardly felt and the level of turbulence is close to null.

This process of diffusion of k from the surface results in a quasi-exponential decay downwards and comes out as a line in the log scale used to plot the vertical profiles. This can be explained by simple analytical developments. If we assume, as shown in the profiles, that the turbulence budget is dominated by the diffusion and dissipation terms, one has:

$$d_4 \sim d_6, \tag{30}$$

i.e.,

$$\frac{\alpha^4 k^2}{\tilde{\nu}} = \frac{\partial}{\partial x_3}\left[\tilde{\nu}\frac{\partial k}{\partial x_3}\right] \tag{31}$$

or

$$\frac{3\alpha^2 k^{3/2}}{2\ell^2} = \frac{\partial^2}{\partial x_3^2} k^{3/2} \tag{32}$$

where a constant mixing length is assumed and where the region of validity of the balance (30) is supposed to extend further than a distance equivalent to the mixing length. The analytical solution is then:

$$k = k_0 \exp\left(\sqrt{\frac{3}{2}}\,\frac{\alpha}{\ell} x_3\right), \tag{33}$$

where k_0 is the turbulent kinetic energy at the surface.

A comparison of this analytical solution with the profiles plotted in Fig. 6 shows that the turbulent kinetic energy could indeed be extrapolated from its surface value to depths of about 60 m, where the turbulent level is negligible, provided that the right (constant) mixing length is used. In this case, at least, the right order of magnitude is predicted and errors in the diffusion coefficient are even smaller (as it depends on the square root of k).

On the north-western European continental shelf, two main sources of turbulence combine to promote much higher turbulent levels: the wind forcing and the tidal stirring. These act, respectively, from the surface and from the bottom, creating two large mixed layers that can combine together in the shallow regions. The vertical structure is therefore very different with possible local maximum of k both at the surface and at the bottom.

While the vertical profiles appears sometimes linear in Fig. 5, the reasons are obviously different from those explained for the Mediterranean Sea case. The dominant balance on the north-western European continental shelf is clearly between the local production and destruction terms while the vertical diffusion plays a less important part. At the bottom, the situation is very close to the local equilibrium. We relied on this hypotheses to derive the bottom

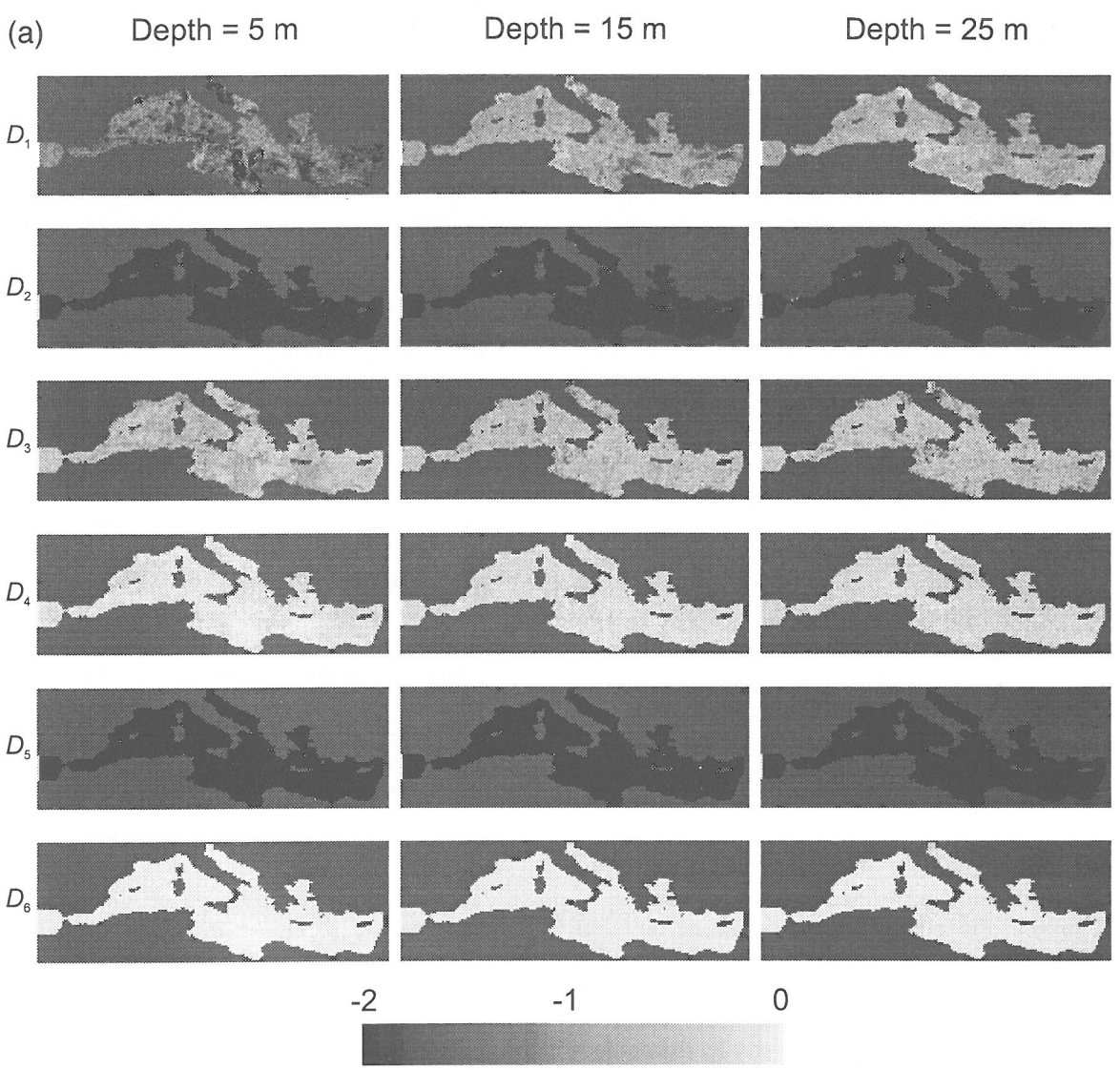

Fig. 4. (a) Horizontal distributions, at 5, 15 and 25 m depth, of the norms of the different terms involved in the equation of k in the Mediterranean Sea in February. (b) Horizontal distributions, at 5, 15 and 25 m depth, of the norms of the different terms involved in the equation of k in the Mediterranean Sea in August.

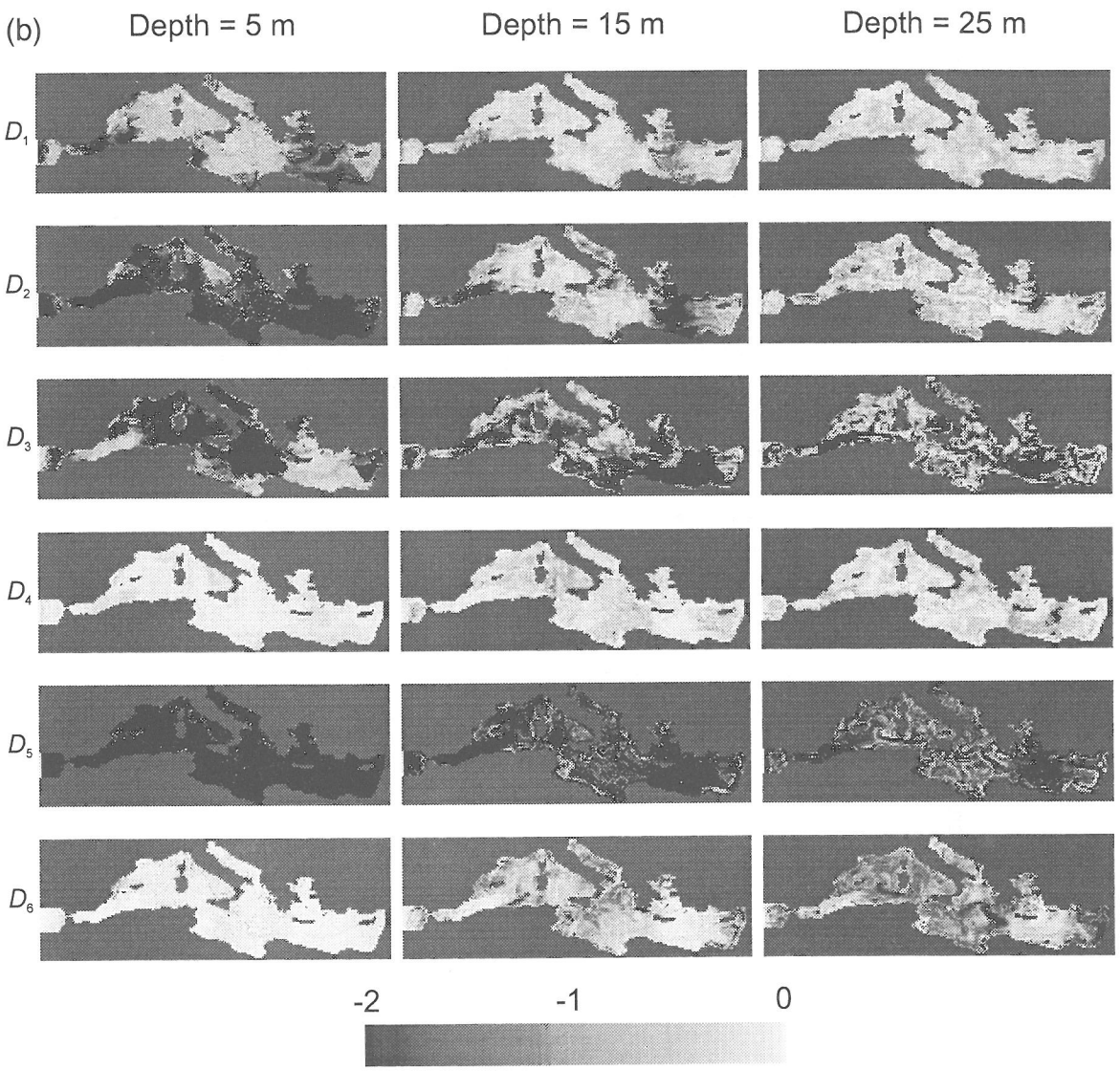

Fig. 4 (*continued*).

boundary condition, and this influences of course the dynamics but it is clear from the vertical profiles that the assumption is compatible with the solution computed at the first grid points above the bottom.

The importance of vertical diffusion increases as the surface is approached, especially at the very high turbulence levels encountered in the English Channel. Vertical diffusion is also important locally both in the surface and bottom layer of the permanently stratified and deeper Norwegian Trench. This area is however not representative of the dynamics of the shelf but much similar to the Mediterranean Sea with the exception of a large production of turbulence in the bottom layer by the interaction of the flow with the steep bathymetry and the trench slope. In this part of the north-western European continental shelf, the precise dynamics of the bottom layer is also poorly resolved because of the larger depth.

The two domains differ also to some extent with respect to the role of advection. In the north-western

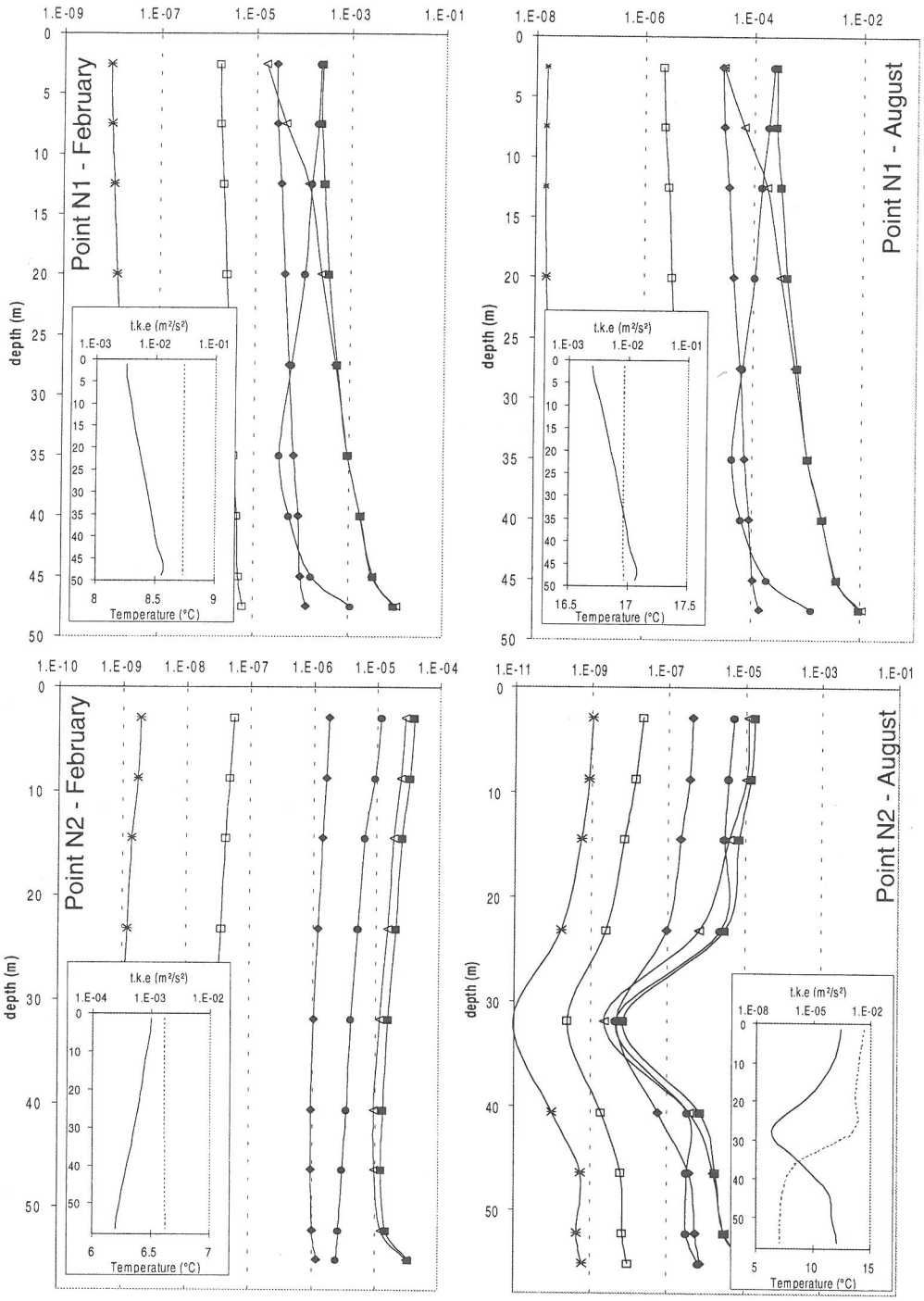

Fig. 5. Vertical profiles at station N1 and N2 on the north-western European continental shelf (see Fig. 1 for location) of the time averaged values of the different terms involved in the equation of k ($\langle d_1 \rangle$ = diamond; $\langle d_2 \rangle$ = empty box; $\langle d_3 \rangle$ = empty triangle; $\langle d_4 \rangle$ = filled box; $\langle d_5 \rangle$ = star; $\langle d_6 \rangle$ = circle) as well as mean k (solid lines) and temperature profiles (dotted lines).

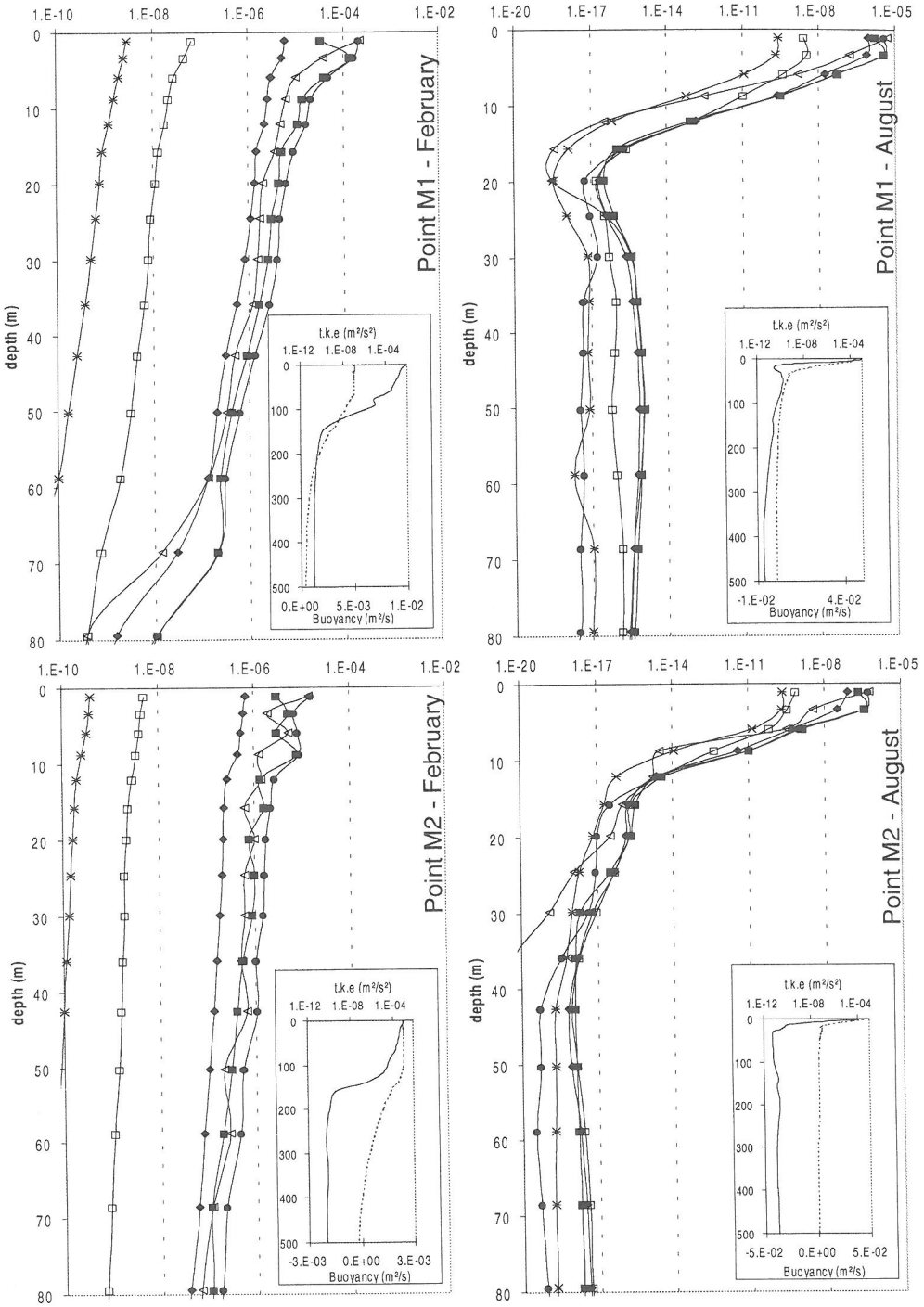

Fig. 6. Vertical profiles at station M1 and M2 in the Mediterranean Sea (see Fig. 2 for location) of the time averaged values of the different terms involved in the equation of k ($\langle d_1 \rangle$ = diamond; $\langle d_2 \rangle$ = empty box; $\langle d_3 \rangle$ = empty triangle; $\langle d_4 \rangle$ = filled box; $\langle d_5 \rangle$ = star; $\langle d_6 \rangle$ = circle) as well as mean k (solid lines) and buoyancy profiles (dotted lines).

European continental shelf, the advection is negligible everywhere even if some local maximum of D_2 are found where large horizontal gradients exists: around capes and headlands, in the vicinity of the slope of the Norwegian Trench. In the Mediterranean Sea model, advection of turbulence is small but turns out to be the dominant mechanism to transfer a tiny part of the turbulent kinetic energy below the thermocline. This turbulence input is very weak and can only sustain a very small turbulence level. As small as it is, this turbulence input might have some implications for those processes occurring at the thermocline or immediately below it as the formation of the deep chlorophyll maximum for instance.

5. Numerical experiments

To verify the conclusions that some terms of the k equation are negligible at large scales, some numerical experiments have been carried out by applying simplified versions of the GHER turbulent closure scheme.

The north-western European continental shelf model was applied to simulate the period from October 1988 to September 1989. This period was chosen because it corresponds with the organisation of the British North Sea Project. During this project, a huge data set was acquired thanks to repeated monthly cruises each lasting 12 days, following the same track and measuring many physical, chemical, biological and sedimentological parameters. The temperature data gathered in the resulting data set offer the possibility to assess the skill of the model in real conditions. Note however that, while the GHER hydrodynamic model covers the whole shelf, the data from the North Sea project are relative only to the Southern Bight of the North Sea (more precisely between the Strait of Dover and 51°N), a region that is stratified only partially during the summer.

To estimate the errors of the simulated temperature field, the numerical results were first interpolated in space to provide model outputs at the actual position and time of the 1398 temperature profiles measured during the North Sea Project. The observed profiles were sampled every meter and contained, therefore, a variable number of data according to the local depth. To give an equal weight to all the profiles, the observed data were aggregated to match the vertical resolution of the model and 10 vertical levels were thus kept at each location. Finally, the mean error and root mean square error were computed for each cruise and for the whole data set. Those errors were computed for both the temperature and the surface–bottom temperature difference. The results are reported in Table 1.

Table 1
Global mean and rms errors (°C) on the temperature and surface-bottom temperature difference. Comparison with the NSP data set

Cruise No.	Dates (1988–1989)	No. of profiles	Error on temperature (°C)		Error on surface–bottom temperature difference	
			MEAN	RMS	MEAN	RMS
37	2/10–14/10	75	1.60	1.76	0.13	0.57
39	1/11–13/11	113	0.94	1.09	0.10	0.30
41	1/12–13/12	70	0.46	0.67	0.03	0.11
43	30/12–12/1	110	0.13	0.48	0.03	0.11
45	28/1–10/2	110	−0.13	0.45	0.04	0.11
47	27/2–12/3	135	−0.18	0.38	0.02	0.07
49	29/3–10/4	89	−0.22	0.40	0.01	0.13
51	27/4–9/5	117	−0.07	0.42	−0.02	0.54
53	26/5–7/6	119	−0.57	1.03	−0.11	1.05
55	24/6–7/7	122	−0.90	1.51	−0.37	1.03
57	24/7–6/8	109	−0.48	1.38	−0.16	1.40
59	23/8–4/9	114	−0.49	1.35	−0.38	1.39
61	21/9–3/10	115	−0.24	0.99	−0.20	1.24
General Statistics		1398	−0.07	1.01	−0.08	0.81

According to these error estimates, there is a good agreement between simulated and observed data. The overall mean error on temperature is about 0.1°C while the RMS error is about 1°C.

It should be noted here that the formulation of the heat flux includes a feedback from the sea to the atmosphere (mainly through the sensible heat flux) that depends on the temperature difference between the two media. Therefore, the simulated heat content is not fully determined by the external forcing data but depends also on the turbulence closure scheme. In this context, the low mean error shows that the total heat content, integrated over the whole North Sea Project domain, is computed accurately. This shows the quality of both the forcing meteorological data, the parameterisation of the heat flux and the computed temperature field.

There is a clear evolution of the accuracy with time. The comparison with the data from cruise 37 shows large errors. This is clearly due to the initialisation of the model. The model run started indeed with climatological data. It is clear from the comparison that these do not reflect the actual situation in October 1988. Afterwards, all the error estimates decrease markedly as the influence of errors on the initial fields diminishes. The best agreement, i.e., the lowest RMS errors, is found for both runs at the beginning of April. Then, with the set-up of the thermal stratification, errors increase. These increased errors can be attributed to the inaccuracies of the turbulent closure schemes but they could also be due to the meteorological data. There is no reason to think that the meteorological data are of poorer quality in summer than in winter and spring, but the sensitivity of the model to the actual meteorological forcing is larger under stratified conditions than under well-mixed conditions.

A detailed analysis of this simulation can be found in (Delhez, 1998). In this paper, the results are also shown to be comparable with those of the more classical Mellor and Yamada 2.5 model.

To go further, the simulations were repeated with three simplified implementations of the GHER turbulence closure scheme:

- run 0 is the standard run with all the terms included in Eq. 4a,b,
- run A is obtained by dropping all the advection and horizontal diffusion terms of k,
- in run B, the time derivative was dropped from the equation for k as well as the advection and horizontal diffusion terms, assuming therefore equilibrium conditions between the local production/destruction terms and the vertical diffusion in the water column,
- in run C, the local equilibrium of k was assumed.

For each of the simulations, the error estimates were re-computed and compared with the error of the standard run. The global figures, for the whole simulated period, are shown in Table 2.

Of course, a more systematic comparison of the different runs could be made and more critical parameters could be examined (like the mixed layer depth for instance). It would, however, certainly be difficult to extrapolate more detailed conclusions to other conditions or other turbulence schemes. With the current approach, it is however clear that while run A is very close to the standard run, (the slight improvement of the mean temperature in run A is obviously fortuitous), the results show a clear deterioration of the results as more processes are omitted in the dynamics of the turbulent kinetic energy., in agreement with the theoretical conclusions drawn above.

Table 2
Global mean and RMS errors (°C) for the different simplified versions of the turbulence closure scheme

	Error on the temperature		Error on the surface–bottom temperature difference	
	MEAN	RMS	MEAN	RMS
Run 0	−0.07	1.01	−0.08	0.81
Run A	−0.08	1.02	−0.08	0.81
Run B	0.04	0.99	−0.28	1.09
Run C	−0.01	1.26	−0.33	1.76

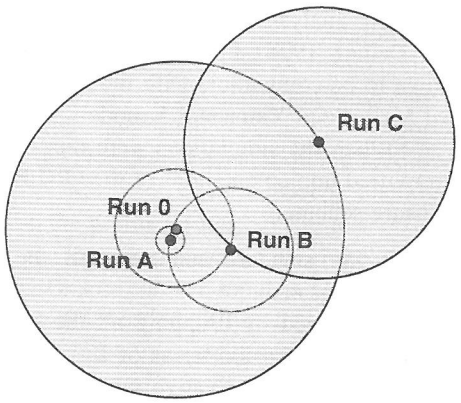

	Run 0	Run A	Run B	Run C
Run 0	-	0.06	0.26	0.75
Run A	0.06	-	0.27	0.76
Run B	0.26	0.27	-	0.6
Run C	0.75	0.76	0.6	-

Fig. 7. Mutual distances (°C) between the temperature fields computed in runs 0, A, B and C and schematic representation.

A graphical illustration of the influence of the simplifications introduced in run A–B–C can further be drawn by computing the distance between the four runs (standard + simplifications) on the basis of the temperature profiles used to compute the error estimates. In Fig. 7, the results of the four simulations can be represented by four points of the plane where the mutual distances between the different points are proportional to the RMS temperature difference between the corresponding runs. The question as whether the additional errors introduced by simplified implementation of the turbulent closure scheme are acceptable or not depend however on the aims and expectations of the model.

6. Concluding remarks

The detailed analysis of the dynamics of turbulence clearly opens the door to possible simplifications of the turbulence closure schemes. This constitutes a first step towards the critical examination of the properties of the scheme that is essential for the understanding of the successes and failures of the whole numerical model.

In the different applications of the GHER hydrodynamic model examined in this paper, the advection and horizontal diffusion terms of k play only a very small part in the dynamics of turbulence and can therefore be neglected unless specific biological systems near the pycnocline are studied. Such a simplification has clear positive consequences on the numerical models using staggered grids. The omission of these terms speaks for the computation of k at the vertical interfaces, where the different eddy diffusivity coefficients are actually needed to represent vertical turbulent fluxes, as the complications introduced by the discretisation of the advection terms is avoided. Neglecting horizontal advection would also allow easier time-splitting for the k equation, since conservation problems due to the velocity divergences in moving grids are eliminated.

The influence of the time derivative is clearly larger than that of the advection and horizontal diffusion terms. Removing this terms from the equation is tantamount to assuming an instantaneous adjustment of turbulence to the hydrodynamic conditions and diffusion, thus neglecting any time-delay in the dynamics of k. Experimental as well as numerical simulations have however highlighted such a delay, for instance, in the tidal regime where the maximum of turbulence occurs shortly after the maximum shear and occurs also later in the middle of the water column that in the bottom layer. This process has some influence on the results as shown in the simulations. The main argument to keep it in the model is however the additional complexity introduced by the numerical determination of the equilibrium value. In practice, the resolution of a stationary equation needs also a solver that is very similar to the usual implicit treatment of a time discretisation. It is, therefore, advisable to keep this in the numerical model unless this introduces unmanageable numerical stability conditions.

The vertical diffusion of k appears as the most significant correction of the local equilibrium assumption. Additional simulations have shown that the mean budget of k over a time scale of several days involves only the local equilibrium between the production and destruction terms, showing that the main effect of the vertical diffusion is to redistribute the turbulent kinetic energy in the water column so that the production and destruction rate patterns do

not match in space but that, in the mean, the local production and destruction rate are close to each other.

The conclusions drawn in this paper about the behaviour of the GHER turbulent closure scheme are obviously conditioned by the hypotheses of the large scale circulation and smoothly varying meteorological forcing functions. The results of a similar analysis carried out at a local scale with rapid wind variations included are likely to be significantly different. With the occurrence of strong horizontal gradients, for instance, horizontal effects will come into play. The design and discretisation of the closure scheme comes, therefore, to the question of whether the model should be universally applicable or optimised for a given study. The option supported by this paper is to apply the most general version of the model in a first step, to diagnose the model, and to identify and implement possible simplifications and optimisations (like the grid staggering) pertinent to the application in mind.

Acknowledgements

Two model intercomparisons supported by the European Union (MEDMEX contract MAS2-CT94-0107 + MAS3-CT96-0051 and NOMADS contract MAS2-CT94-010X + MAS3-CT98-0163) lead to some of the questions addressed in the present paper. The authors gratefully acknowledge the E.U. support. M. Grégoire and J.-M. Beckers are indebted to the National Fund for Scientific Research of Belgium for its support.

References

Beckers, J.-M., 1991. Application of a 3D model to the Western Mediterranean. Journal of Marine Systems 1, 315–332.

MEDMEX, Beckers, J.-M., 1998. Model intercomparison in the Mediterranean. The MEDMEX simulations of the seasonal cycle. Journal of Marine Systems, in preparation.

Brasseur, P., Brankart, J.-M., Schoenauen, R., Beckers, J.-M., 1996. Seasonal temperature and salinity fields in the Mediterranean Sea: climatological analysis of a historical data set. Deep Sea Research 43, 159–192.

Burchard, H., Petersen, O., 1999. Models of turbulence in the marine environment—a comparative study of two-equation turbulence models. Journal of Marine Systems 21, 29–53.

Davies, A.M., Jones, J.E., 1990. Application of three-dimensional turbulence energy model to the determination of tidal currents on the Northwest European shelf. J. Geophys. Res. 95 (10), 18143–18162.

Davies, A.M., Luyten, P.J., Deleersnijder, E., 1995. Turbulence energy models in shallow sea oceanography. In: Quantitative Skill Assessment for Coastal Ocean Models. Lynch, D.R., Davies, A.M. (Eds.), Coastal and Estuarine Studies 47 American Geophysical Union, pp. 97–123.

Deleersnijder, E., Luyten, P., 1994. On the practical advantages of the quasi-equilibrium version of the Mellor and Yamada level 2.5 turbulence closure applied to marine modelling. Applied Math. Modelling 18, 281–287.

Deleersnijder, E., Nihoul, J.C.J., 1988. Turbulent fields associated with the general circulation in the northern Bering Sea. In: Nihoul, J.C.J., Jamart, B.M. (Eds.), Small scale turbulence and mixing in the ocean. Elsevier, Amsterdam, pp. 73–93.

Delhez, E.J.M., 1998. Modelling marine turbulence. Physicalia Mag. 4, 355–370.

Grégoire, M.L., Beckers, J.-M., Nihoul, J.C.J., Stanev, E., 1998. Reconnaissance of the main Black Sea's ecohydrodynamics by means of a 3D interdisciplinary model. Journal of Marine Systems 16, 85–105.

Jaeger, L., 1976. Monthly precipitation maps for the entire earth. Ber. Deutschen Wetterdienstes 18, 38 pp. (in German).

Kitaigorodskii, S.A., 1979. Review of the theories of wind-mixes layer deepening. In: Nihoul, J.C.J. (Ed.), Marine Forcasting. Elsevier, Amsterdam, pp. 1–33.

Luyten, P.J., Deleersnijder, E., Ozer, J., Ruddick, K.G., 1996. Presentation of a family of turbulence closure models for stratified shallow flows and preliminary application to the Rhine outflow region. Continental Shelf Research 16, 101–130.

Martin, G., Delhez, E.J.M., 1994. 3D turbulence fields on the Northwest European Continental Shelf. Tellus 46A, 98–112.

Mellor, G., Yamada, T., 1982. Development of a turbulence closure model for geophysical fluid problems. Rev. Geophys. 20, 851–875.

Nihoul, J.C.J., 1993. Application of mathematical modelling to the marine environment. In: Zanetti, P. (Ed.), Environmental Modeling I Computational Mechanics Publications, Ashurst, Hants, England, pp. 75–140.

Nihoul, J.C.J., Deleersnijder, E., Djenidi, S., 1989. Modelling the general circulation of shelf seas by 3D $k-\varepsilon$ models. Earth Science Reviews 26, 163–189.

Ozmidov, R.A., 1967. The dependence of the horizontal turbulent exchange coefficient in the ocean on the scale of the phenomenon. Izv. Atmos. Oceanic Phys. Series 4, 1224–1225.

Rodi, W., 1980. Turbulence models and their application in hydraulics, IAHR Publishing, Delft.

Rodi, W., 1987. Examples of calculation methods for flow and mixing in stratified fluids. J. Geophys. Res. 92, 5305–5328.

Ruddick, K.G., Deleersnijder, E., Luyten, P.J., Ozer, J., 1995. Haline stratification in the Rhine–Meuse freshwater plume: a three-dimensional model sensitivity analysis. Continental Shelf Research 15 (13), 1597–1630.

Varela, R.A., Cruzado, A., Tintoré, J., Ladona, E., 1992. Modelling the deep-chlorophyll maximum: a coupled physical–biological approach. Journal of Marine Research 50, 441–463.